BSTS Synthesis Guided by CALPHAD Approach for Phase Equilibria and Process Optimization

Husain F. Alnaser and Taylor D. Sparks*

Dept. of Material Science and Engineering, University of Utah, Salt Lake City, UT 84112, USA *Corresponding author: sparks@eng.utah.edu

Abstract:

This work presents a new method for processing single crystal semiconductors designed by a computational method to lower the process temperature. This research study is based on a CALPHAD approach (Thermo-Calc) to theoretically design processing parameters by utilizing theoretical phase diagrams. The targeted material composition consists of Bi–Se₂–Te–Sb (BSTS). The semiconductor alloy contains three phases, hexagonal, rhombohedral-1, and rhombohedral-2 crystal structures, that are presented in the phase field of the theoretical pseudobinary phase diagrams. The semiconductor is also evaluated by applying Hume-Rothery rules along with the CALPHAD approach. This method yields promising results suggesting the possibility of significantly lower temperature single crystal growth of BSTS at 350°C. The evaluation extends to include identification of phase equilibria such as solidus lines, liquidus lines, solubility limits, and chemical reaction points.

Keywords: BSTS, single crystal, CALPHAD, thermodynamic modeling.

Introduction:

Using topological insulating materials for quantum computing is a promising emerging technology that will have vast implications on industry and society as a whole [1]. For decades, computers have been developed to be smaller in size, faster in operation, and larger in memory size [2]. However, as transistors reach the nanometer scale, low dimensional phenomena such as tunneling become more problematic, and radical alternative approaches, such as quantum

computing, must be considered. Quantum-matter heterostructures have emerged as a versatile approach for controlling quantum states in materials [2].

Advanced semiconductor devices use heterostructure as a building block because of the precise control over the states and motions of charge carriers. The heterostructure advantages stem from harvesting a unique design where a thin layer of material grows on a different thin layer of material that has different bandgaps and lattice constants providing an easy tunneling effect for the carriers to promote quantum wells [3]. The heterostructure can be synthesized by an epitaxial growth process such as molecular beam epitaxy, liquid phase epitaxy, and chemical vapor deposition. In our previous studies, BiSbTeSe₂ (BSTS) alloy was proven to be an excellent candidate for a 3D topological insulator utilizing the heterostructure approach because each layer provides a unique set of properties that when combined promote the quantum hall effect [4-6]. The theoretical predictions suggest that the interior of a topological insulator material sample works like an insulator, while the exterior, namely, the metallic surface, has a Dirac cone dispersion and a helical spin structure [7]. Despite the availability of other compounds that serve as a good topological insulator, BSTS was favored because it provides a stable platform for characterizing without disturbing the bulk electron states [8].

Quantum computers need special topological insulator materials to optimize their capacity ^[9]. BSTS single crystals have drawn researchers' attention because of the Dirac quantum hall effect ^[10]. Consequently, BSTS single crystals have been studied by many researchers because they offer unmatched opportunities for creating new novel quantum state possibilities ^[11]. The manufacture of quantum-matter heterostructures relies on the exfoliation of thin sections of high-quality materials, such as single crystals ^[12]. Many researchers have attempted to make BSTS single crystals through trial-and-error high-temperature synthesis. To

date, there are only limited reports of process design principles despite the requirement for improved purity, control of composition, larger crystals, and reduced energy consumption upon synthesis.

In other fields such as solid-solution strengthening, thermodynamic modeling is used regularly to guide synthesis and provide process design principles [13]. For example, the simple Hume-Rothery rules provide a starting point for alloy design via solid-solution strengthening. The four rules are: If the solute is more than 15% different in size from the solvent, the solubility of the species is limited. If the solute has a large difference in electronegativity, then the solvent forms intermetallic compounds and limits the alloy solubility. If the solute and the solvent have the same valence, complete solubility occurs; otherwise, solubility would be limited. Lastly, if the solute and solvent have different crystal structures, then solubility would be limited. These rules work best for binary alloys but can be extended to even more complex systems if these are treated as a pseudo-binary alloy where the composition is held constant (the solvent) except for the addition of one constituent (the dopant). The generation of pseudo-binary diagrams is nontrivial and relies on the aid of thermodynamic modeling such as CALPHAD (Computer Coupling of Phase Diagrams and Thermochemistry) Thermo-Calc software. CALPHAD allows researchers to compute thermochemical properties and phase diagrams [14]. These computations are precise and accurate to a high degree. A study performed by Fetzer comparing the phase diagrams of experimental data versus the CALPHAD approach to determine the precession of thermodynamic properties and phase fields for Mg alloys. He concluded that the CALPHAD approach precisely predicted his experimental data [15].

Polycrystalline materials have limits and cannot perform as required because of the formation of grain boundaries that reduce electron mobility because of electrostatic potentials

and lattice mismatch ^[16]. Grain boundaries are also susceptible to enhanced corrosion because of their higher energy state. Single crystals, on the other hand, have excellent corrosion resistance and enhanced electronic mobility that have made these materials staples for modern semiconductor industries ^[17]. Topological insulator single crystals have recently been employed in heterostructure architectures because of enhanced electron transport, control of specific crystal orientation, and interfaces ^[18]. The synthetic techniques used for these topological insulating single crystals are quite varied and span zone melting, Czochralski method, Bridgman method, saturated solution growth, flux method, and others ^[19].

The literature review shows that a common temperature for single crystal growth of BSTS is in excess of 850°C without thermodynamic justification ^[20-21]. BSTS is composed of several toxic elements with dangerous health implications for those exposed ^[22-25]. Consequently, relying on a high-temperature synthesis route has potential disadvantages because of the ease of contamination that is possible because of the excessive volatilization of low-melting-point constituents. In addition, most single crystal growers use quartz ampoules to isolate the BSTS materials from oxidation during crystal growth, and tube rupture is a regular concern. A tuberupture formula can determine the ampoule thickness needed to withstand the internal pressure generated because of interior component volatilization ^[26]. Note that the formula cannot be used when the internal pressure exceeds 100 psi = 6.89 bar.

The boiling point of Se is 685°C; therefore, increasing the temperature up to 850°C causes the partial pressure to increase inside the ampoule, making it a pressurized vessel and a fire hazard. Figure 1 presents theoretical data for BSTS elements and their partial pressure while varying the temperature described by Clausius–Clapeyron equation [27-29]. The Se partial pressure after 650°C is very large, while the partial pressure of Se at 850°C is 5.9 bar, which is equal to

85.57 psi and very close to the boundaries of the internal pressure ampule formula with a value of 6.8 bar resembled by the critical point line in red. A potential solution is to have a thicker ampoule wall to sustain the pressure, but the pressure that the ampoule would withstand needs to be calculated to ensure it passes the safety requirement for the growth. Even so, a thicker ampoule still would be pressurized, meaning the hazard still exists, and upon failure, the results would be catastrophic. Thus, the main recommendation is to lower the processing temperature, preventing pressure from increasing inside the ampoule without losing efficiency or increasing growth time, but to date, no recommendations exist for what temperatures would satisfy the thermodynamic growth requirements for BSTS.

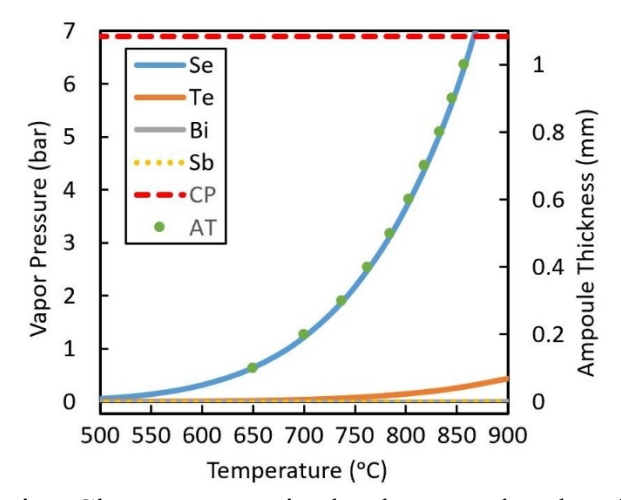


Figure 1: The Clausius–Clapeyron equation has been used to describe the relationship between temperature and vapor pressure for the BSTS system elements starting from 500°C to 900°C with ampoule thickness as a third axis. (CP) is the critical point at which the ampoule equation limits at and (AT) is the ampoule thickness of quartz tube.

In this work, we set out to establish design principles for growing BSTS at low temperatures by leveraging thermodynamic modeling. We hypothesized that it is possible to grow high-quality BSTS single crystals at lower temperatures and that this modeling approach can be used to better understand how the elements interact with each other and form the compound(s) of interest. We show that growth conditions can be reduced from 850°C to as low as 350°C. Moreover, we show that this lower temperature processing route can provide better control over composition and therefore a higher quality BSTS single crystal under safer conditions because of reduced Se volatilization.

Methods

ThermoCalc. Psedo-binary phase diagrams were constructed for the BSTS system with a fixed ratio of 1:1:1:2 for the elements Bi-Sb-Te-Se respectively. Specifying the condition at which the material to be grown (temperature from 0° to 650° with 1 ATM and composition from 0% to 30% because our composition lies on a 10% line for Bi-Sb-Te and 20% for Se). The program then runs the calculation for the binary subsystems (Bi-Sb, Bi-Se, Bi-Te, Sb-Se, Sb-Te, Te-Se) crossing the data with Gibbs free energy data to create the final result as a pseudo-binary phase diagram where the ratio of the elements is fixed except for one element where it will help to draw the phases as a function of composition vs temperature.

The property model calculator predicts material properties based on their chemical composition and temperature. The calculator can compute the driving force, interfacial energy, liquids and solidus temperature, amount of phases, and phases activities, thus graphing the properties as contour plots or thermal maps [31]. For the BSTS alloy, the interest was to calculate Gibbs' energy of formation plotted as a thermal map and amount of phase formation plotted as a contour plot. Any desired property would be calculated and shown as a third axis while the main

calculation would be done as a function of temperature versus composition. For convenience, all properties are shown by selecting the temperature to be from 0° to 600° while varying Bi mole%.

The Hume-Rothery four rules of solid-solution strengthening evaluation were utilized for the BSTS alloy where each pair of elements were evaluated (Bi-Sb, Bi-Se, Bi-Te, Sb-Se, Sb-Te, Te-Se). Moreover, The Clausius-Clapeyron equation has been used to describe the relationship between temperature and vapor pressure for the BSTS system $\ln \left(\frac{P_1}{P_2} \right) = \frac{-\Delta H_{vap}}{R}$ $\left(\frac{1}{T_1} - \frac{1}{T_2}\right)$, where P₁ is the known vapor pressure at a known temperature in (atm), P₂ is the vapor pressure of interest in (atm), T_1 is the corresponding temperature for P_1 in (K), T_2 is the temperature of the point of interest in (K), ΔH_{vap} is the enthalpy of vaporization in J/mol and R is the universal gas constant 8.314 J/(mol*K). The following is an example calculation of Se vapor pressure at 700°C. The known temperature and pressure at the Se melting point are $T_1 = 494 \text{ K}$ and $P_1 = 1.283e-5$ atm, respectively. Converting the temperature of interest from Celsius to Kelvin yields $T_2 = 973$ K. The heat of vaporization is $\Delta H_{vap} = 95480$ J/mol, and the gas constant is R = 8.314 J/(mol*K). Solving for P₂, P₂= 1.2 atm = 1.22 bar. $\ln \left(\frac{1.283e - 5}{P_2} \right) = \frac{-95480}{8.314}$ $\left(\frac{1}{494} - \frac{1}{973}\right)$, solving for P_2 , $P_2 = 1.2$ atm = 1.22 bar. In addition, the internal pressure of an ampoule formula is $S = \frac{P * r}{t}$, where S is hoop stress in (Pa), P is working pressure in (Pa), r is inside radius of the ampule (mm) and t is ampoule wall thickness.

Scheil simulation is a solidification calculator for estimating the solidification range of an alloy and the phases formed at various temperatures shown as a contour plot. It offers a precise prediction of the diffusion in the solid state, solidification range of an alloy, phase formation, and composition in comparison to equilibrium solidification calculation. The plot is usually used

heavily in steel-making processes. Also, it can calculate the alloy segregation profile as a composition concentration gradient from the liquid phase to the solid phase. The equation used is $C_s = k * C_0 (1 - f_s)^{k-1}$, where C_s is the concentration of solute in the solid, C_0 is the initial concentration of the liquid. f_s is the fraction solidified and k is the partition coefficient.

Results and Discussion

BSTS is a quaternary alloy that has been analyzed based on the Hume-Rothery rules. The evaluation of all binary systems of the BSTS yielded 33.3%, meaning that the BSTS alloy results in a multiphase alloy that in terms of a solid solution, strengthening is unfavorable because multiphases tend to make the material brittle. However, the alloy was designed intentionally in a way to utilize the multiphase structure to create a semiconductor material that has a property of a conductor through the bulk and an insulator on the surface. Table 1 shows the elemental properties that are necessary for the evaluation starting with atomic size [32]. The atomic size difference criteria for the BSTS alloy is 50% in favor of solid-solution strengthening where the binary alloys of BSTS (Bi-Te, Bi-Sb, Te-Sb) have satisfied the condition where the atomic size difference must be less than 15%. The crystal structure criteria for the BSTS alloy is 33.3% in favor of solid-solution strengthening. The crystal structure of Bi is the same as Sb, indicating high solubility can occur, and the same is true for Te and Se. However, limited solubility occurs between Bi(Te,Se) binary alloys, and the same is true for Sb(Te,Se) binary alloys because of crystal structure differences. The valence criteria for the BSTS alloy is 33.3% in favor of solidsolution strengthening. The valence of the BSTS elements has the same conclusion as crystal structure criteria on predicting and evaluating solid-solution strengthening where Bi and Sb have the same valence and Te and Se have the same valence. However, Bi(Te,Se), Sb(Te,Se) binary

alloys have different valences that limit solubility. Lastly, large differences in electronegativity cause intermetallic phase formation that limits the solubility between elements. The electronegativities of the BSTS elements are marginally different and dictate that solubility is limited, resulting in multiphase formation. The binary phase diagrams presented in Figure 2 have been constructed by the CALPHAD approach to aid in evaluating the electronegativity criteria and to identify the possible phases. The results are summarized as follows: all species are going to form two phases (hexagonal-rhombohedral) except for the Te—Se binary forming one phase (trigonal).

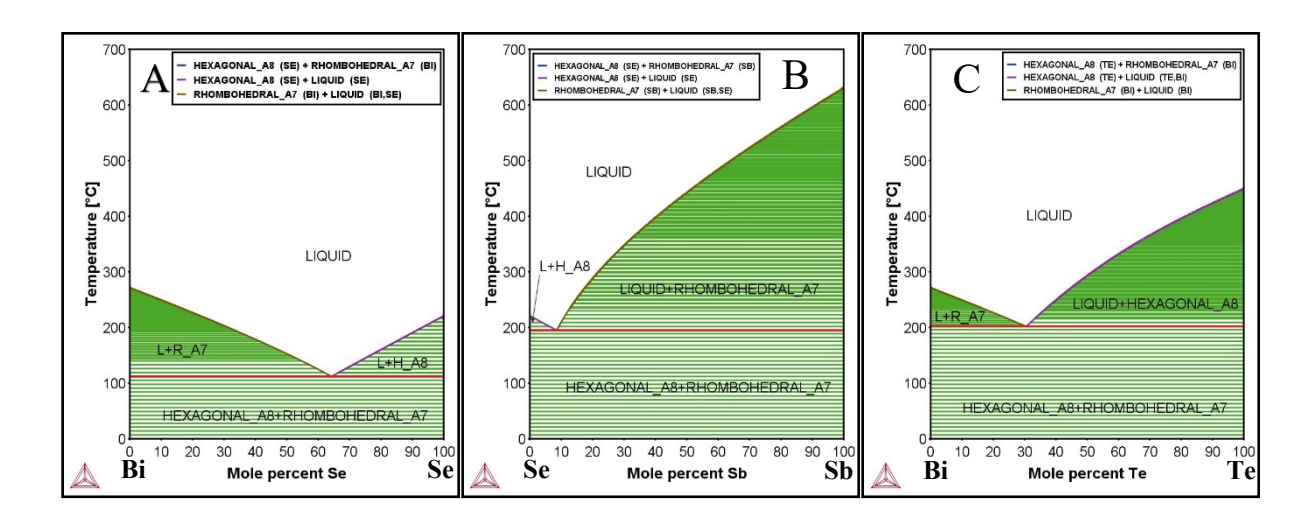
Thus, Hume-Rothery rules predict that BSTS has poor solubility and leads to an alloy that contains multiphases. The possible phases that the binary phase diagrams suggested are hexagonal, rhombohedral, and trigonal. However, our system is quaternary and therefore we must construct pseudo-binary phase diagram as opposed to simple binary phase diagram.

Table 1: BSTS elements and their properties, where El is the elements, AR is the atomic radius, CR is the crystal structure, V is the valance, EN is the electronegativity, Rhom is the rhombohedral crystal structure, and Hex is the hexagonal crystal structure.

Hume-Rothery Rules												
Physical Properties					Atomic Size Difference %				Intermetallic Compound Formation			
E1	AR (pm)	CS	V	EN	Bi	Te	Se	Sb	Bi	Te	Se	Sb
Bi	155	Rhom	3	1.9	0	7.7	25.2	6.5	All binaries have two phases except Te-Se has one phase			
Te	143	Hex	4	2.1	7.7	0	18.9	1.4				
Se	116	Hex	4	2.55	25.2	18.9	0	20				
Sb	145	Rhom	3	2.05	6.5	1.4	20	0				

Binary phase diagrams of the BSTS alloy have been created to provide a fundamental understanding of the reactions of the elements with each other. As a common metallurgical

process concept, it is highly practiced that the alloy made is engineered to target the eutectic point where the elements will liquefy and get mixed lowering the temperature of the mixture melting point along the liquids line, as shown in some of the diagrams presented in Figure 2. Figure 2A, 2B, 2C and 2D are all simple eutectic binary phase diagrams with a eutectic temperature of 112°C, 200°C, 205°C and 363°C respectively suggesting a minimum processing temperature be above the eutectic point. Moreover, the stable phase field at room temperature is containing hexagonal and rhombohedral phases. Figure 2E has a spinodal decomposition phase filed slightly shifted to the right in favor of Sb content having two phases of rhombohedral. Above it the alloy has one rhombohedral phase. Figure 2F resembling an isomorphous phase diagram with a trigonal crystal structure. In addition, the gas phase form because of Se evaporation at roughly 688°C when having an alloy rich in Se. Hence, processing the sample at 850°C can alter the stoichiometric ratio of the BSTS compound because of the higher probability of gas formation mainly from Se. Therefore, 650°C should be the maximum operating temperature.



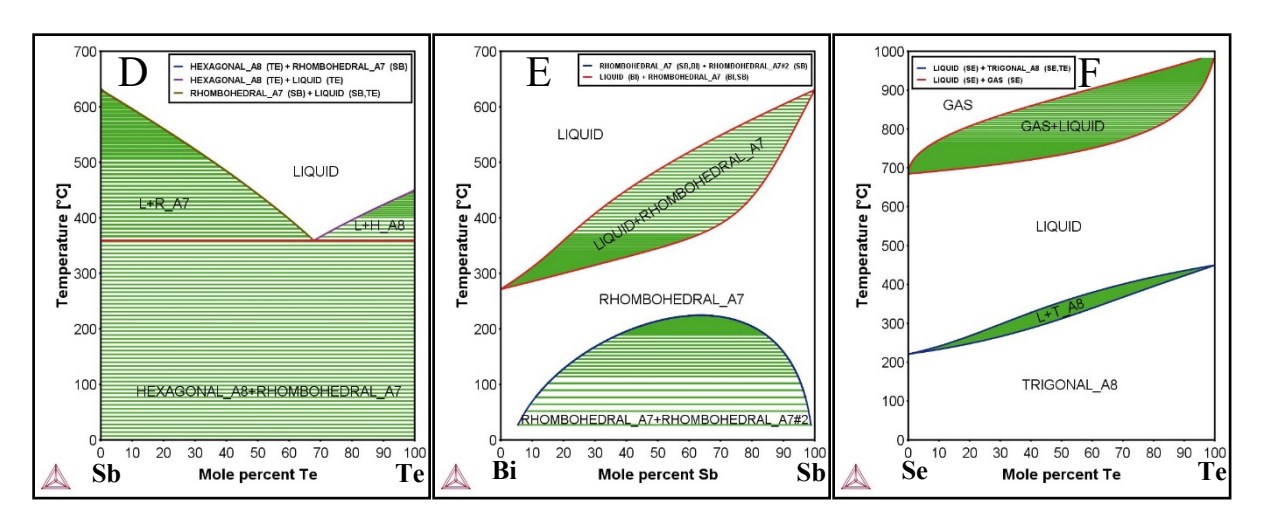


Figure 2: Binary phase diagrams of the BSTS alloy. A binary phase diagram of (Bi–Se), B binary phase diagram of (Se–Sb), C binary phase diagram of (Bi–Te), D binary phase diagram of (Sb–Te), E binary phase diagram of (Bi–Sb) and F binary phase diagram of (Se–Te).

The analysis sequence started with constructing pseudo-binary phase diagrams followed by thermal mapping of thermodynamic properties of the phases created. The pseudo-binary phase diagrams can be analyzed to visually show the liquidus line that the crystal growth can start from. In addition, the graphs will indicate the stable phase at room temperature for the given composition of BSTS. Analysis of the pseudo-binary BSTS diagram shows a temperature of as low as 350°C where a single liquid phase exists. Therefore, single crystal growth could be achieved thermodynamically at 350°C as opposed to higher temperature. The analysis of all four pseudo-binary phase diagrams suggest that the stable phases at room temperature are hexagonal and two rhombohedral phases. Figure 3 presents the pseudo-binary phase diagrams where the initial parameters of temperature, pressure, and composition were modeled by Thermo-Calc software in accordance with the lab environment (P = 1 atm, T = 25°C) where the red vertical line represents the composition with a Bi–Sb–Te–Se ratio of 1:1:1:2.

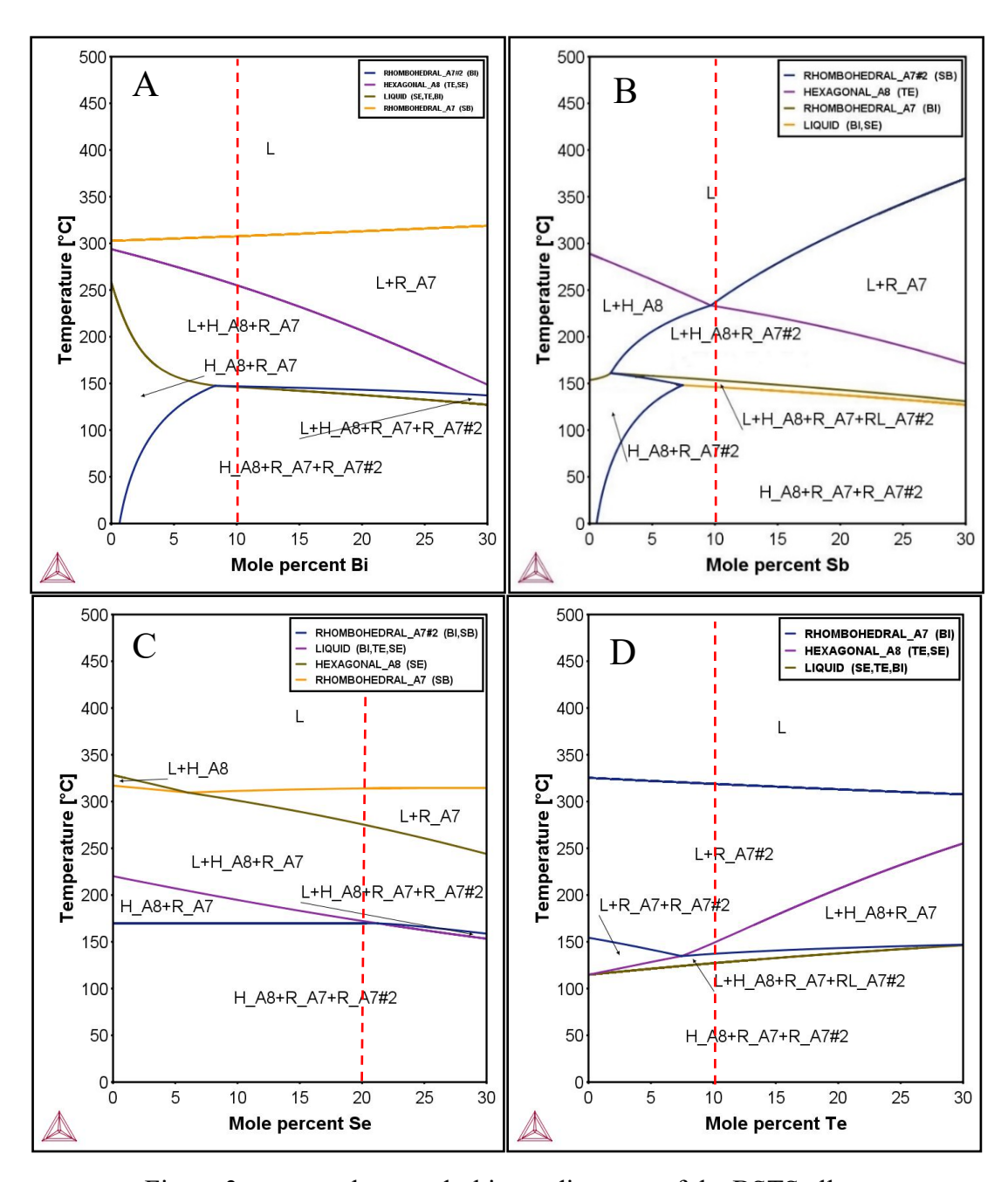


Figure 3 presents the pseudo-binary diagrams of the BSTS alloy.

Clearly the pseudo-binary phase diagrams suggest that from a thermodynamic stand point multiple phases should form when growing the BSTS ratio of 1:1:1:2. Nevertheless, previous reports including our own all reported of a single phase of a BSTS single crystal. Therefore, it can be assumed that kinetics playing a substantial rule in formation of a phase over others.

Indeed, our analysis of gibs free energy of different phases shows very different stabilities for the phases hexagonal, rombahedral-1, and rhombahedral-2. Figure 4 shows thermal map of Gibbs energy for the BSTS. For example, at 300°C, the hexagonal phase Gibbs energy is about –700 kJ, as shown in Figure 4A, whereas the rhombohedral phase Gibbs free energy at the same temperature is about –175 kJ, as shown in Figure 4B. therefore, the hexagonal phase is four times more likely to form than the rhombohedral phase and could explain the sluggish kinetics of these competing phases as well as the growth of the hexagonal phase in the final crystal, growth is dictated by the kinetics factor which ultimately explain the growth of phase over the over.

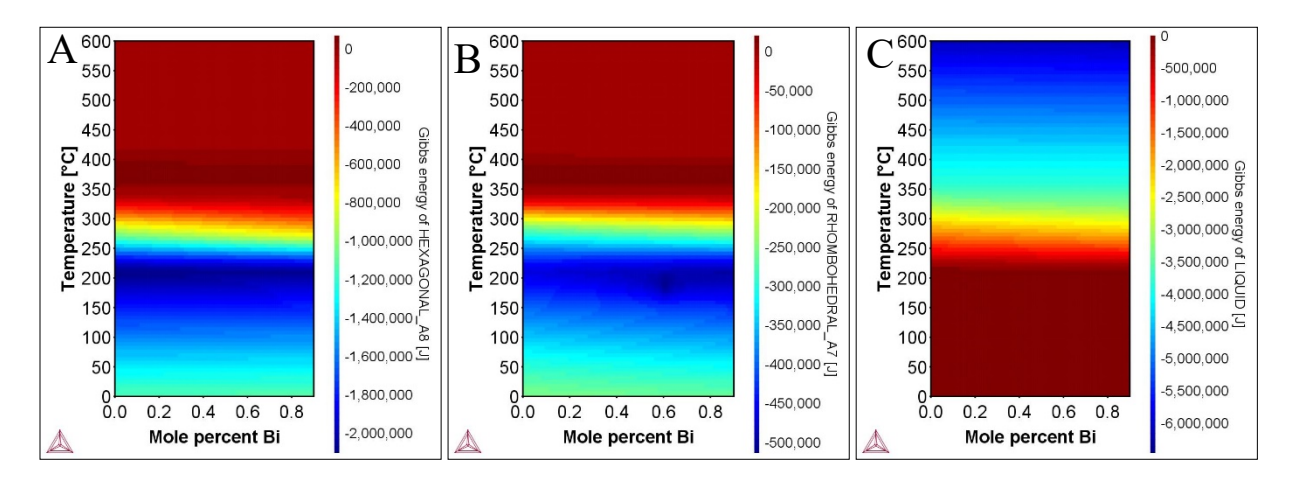


Figure 4: Thermal map of Gibbs free energy for the BSTS phases through various temperatures.

The phase concentrations present at room temperature are found to be approximately around 70% hexagonal and 30% rhombohedral. It may perhaps be observed without straying too far afield from our primary focus that in experimental practice, this mixture of phases is avoided regularly. Very often, single phase growth is achieved. In our previous study done by Kyu et al., it has been ascertained that the single crystal grown has a rhombohedral crystal structure with space group R3m^[33]. Figure 5A shows the concentrations of phases created under various temperature ranges. Also, the graph shows exactly the starting/ending point of a phase. Notedly, it indicates that some liquid will form around 125°C and that the liquid amount is approximately

20% around 150°C. However, for single crystal growth, the required starting amount of liquid needs to be 100%. In this study, Scheil simulation was used to show the critical point at which the phase starts to micro-segregate to form a solid phase in BSTS alloy [34-35]. Figure 5B shows interesting results. For example, starting at 320°C, a full liquid BSTS forms a rhombohedral phase when cooled (red line), and during the cooling process, no sign of segregation is observed. At about 200°C, a new phase forms and a small deviation occurs, separating the equilibrium line from the phase line where the micro-segregation starts (green line). The behavior of solidification changes around a 0.5 mole fraction nearly at 140°C because the increase in hexagonal phase stability is roughly equal to six times the rhombohedral phase according to Gibbs free energy diagrams, where at higher temperatures it was around four times, as mentioned previously.

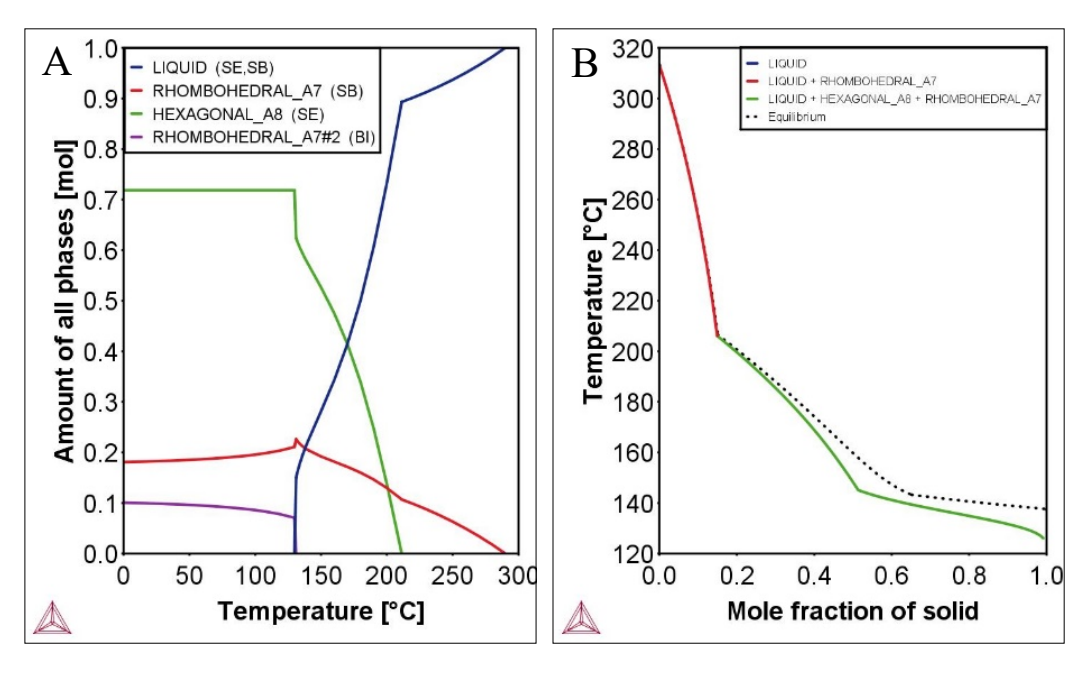


Figure 5: Material phase properties of BSTS. Figure 5A contour plot of the phase concentrations vs temperature. Figure 5B Scheil simulation.

Conclusion

- Hume-Rothery rules can predict solid-solution homogeneity formation accurately for binary alloys. Any elements can be used as substitutional elements or added to the mix once they follow the rules to predict their behavior. As for complex alloys, more methods such as the CALPHAD approach are needed to empower prediction accuracy.
- CALPHAD approach has been used to determine the optimum conditions theoretically
 for BSTS single crystal growth and has given valuable insights about dominant phases
 and their quantity.
- Scheil simulation provides an overview of the BSTS solidification process.

Acknowledgements

• This work was supported by the KFAS GRF program at the University of Utah under grant # 10059664, CB20-68EO-01, and the NSF QII-TAQS grant # 1936383.

References

- 1- Bhat, H. L. Introduction to Crystal Growth: Principles and Practice, Taylor & Francis Group, 2014. ProQuest Ebook Central, https://ebookcentral-proquest-com.ezproxy.lib.utah.edu/lib/utah/detail.action?docID=1687634.
- 2- Boschker, H., and J. Mannhart. "Quantum-Matter Heterostructures." Annual Review of Condensed Matter Physics, vol. 8, no. 1, 2017, pp. 145–64. Crossref, doi:10.1146/annurev-conmatphys-031016-025404.
- 3- Einspruch, Norman, and William Frensley. "Chapter 1 Heterostructure and Quantum Well Physics." Heterostructures and Quantum Devices (ISSN Book 24), 1st ed., Academic Press, 2014, pp. 1–24.

- 4- Chong, Su Kong, et al. "Tunable Coupling between Surface States of a Three-Dimensional Topological Insulator in the Quantum Hall Regime." Physical Review Letters, vol. 123, no. 3, 2019. Crossref, doi:10.1103/physrevlett.123.036804.
- 5- Chong, Su Kong, et al. "Topological Insulator-Based van Der Waals Heterostructures for Effective Control of Massless and Massive Dirac Fermions." Nano Letters, vol. 18, no. 12, 2018, pp. 8047–53. Crossref, doi:10.1021/acs.nanolett.8b04291.
- 6- Chong, Su Kong, et al. "Landau Levels of Topologically-Protected Surface States Probed by Dual-Gated Quantum Capacitance." ACS Nano, vol. 14, no. 1, 2019, pp. 1158–65.

 Crossref, doi:10.1021/acsnano.9b09192.
- 7- Xia, B., et al. "Anisotropic Magnetoresistance in Topological Insulator
 Bi1.5Sb0.5Te1.8Se1.2/CoFe Heterostructures." AIP Advances, vol. 2, no. 4, 2012, p.
 042171. Crossref, doi:10.1063/1.4769894.
- 8- Ren, Zhi, et al. "Large Bulk Resistivity and Surface Quantum Oscillations in the Topological InsulatorBi2Te2Se." Physical Review B, vol. 82, no. 24, 2010. Crossref, doi:10.1103/physrevb.82.241306.
- 9- Xu, Yang, et al. "Observation of Topological Surface State Quantum Hall Effect in an Intrinsic Three-Dimensional Topological Insulator." Nature Physics, vol. 10, no. 12, 2014, pp. 956–63. Crossref, doi:10.1038/nphys3140.
- 10-Pan, Y, et al. "Low Carrier Concentration Crystals of the Topological Insulator Bi2-xSbxTe3-YSey: a Magnetotransport Study." New Journal of Physics, vol. 16, no. 12, 2014, p. 123035., doi:10.1088/1367-2630/16/12/123035.

- 11- Kushwaha, S. K., et al. "Sn-Doped Bi1.1Sb0.9Te2S Bulk Crystal Topological Insulator with Excellent Properties." Nature Communications, vol. 7, no. 1, 2016. Crossref, doi:10.1038/ncomms11456.
- 12- Wangyang, Peihua, et al. "Mechanical Exfoliation and Raman Spectra of Ultrathin PbI2 Single Crystal." Materials Letters, vol. 168, 2016, pp. 68–71. Crossref, doi:10.1016/j.matlet.2016.01.034.
- 13- Smith, William, and Javad Hashemi. Foundations of Materials Science and Engineering.6th ed., McGraw-Hill Education, 2018.
- 14-Lukas, Hans. Computational Thermodynamics: The Calphad Method. 1st ed., Cambridge University Press, 2007.
- 15- Schmid-Fetzer, R., and J. Gröbner. "Focused Development of Magnesium Alloys Using the Calphad Approach." Advanced Engineering Materials, vol. 3, no. 12, 2001, p. 947. Crossref, doi:10.1002/1527-2648(200112)3:12<947::AID-ADEM947>3.0.CO;2-P.
- 16-Mao, W. G., et al. "Deformation Behavior and Mechanical Properties of Polycrystalline and Single Crystal Alumina during Nanoindentation." Scripta Materialia, vol. 65, no. 2, 2011, pp. 127–30. Crossref, doi:10.1016/j.scriptamat.2011.03.022.
- 17- Toyoda, Taro, et al. "The Electronic Structure and Photoinduced Electron Transfer Rate of CdSe Quantum Dots on Single Crystal Rutile TiO2: Dependence on the Crystal Orientation of the Substrate." The Journal of Physical Chemistry C, vol. 120, no. 4, 2016, pp. 2047–57. Crossref, doi:10.1021/acs.jpcc.5b09528.
- 18- Analytis, James G., et al. "Two-Dimensional Surface State in the Quantum Limit of a Topological Insulator." Nature Physics, vol. 6, no. 12, 2010, pp. 960–64. Crossref, doi:10.1038/nphys1861.

- 19- Crystal Growth of Intermetallics, edited by Peter Gille, and Yuri Grin, Walter de Gruyter GmbH, 2018. ProQuest Ebook Central, https://ebookcentral-proquest-com.ezproxy.lib.utah.edu/lib/utah/detail.action?docID=5157992.
- 20- Ren, Zhi, et al. "Optimizing Bi2–xSbxTe3–ySey Solid Solutions to Approach the Intrinsic Topological Insulator Regime." Physical Review B, vol. 84, no. 16, 2011. Crossref, doi:10.1103/physrevb.84.165311.
- 21- Taskin, A. A., et al. "Observation of Dirac Holes and Electrons in a Topological Insulator." Physical Review Letters, vol. 107, no. 1, 2011. Crossref, doi:10.1103/physrevlett.107.016801.
- 22- MacFarquhar, Jennifer K. "Acute Selenium Toxicity Associated With a Dietary Supplement." Archives of Internal Medicine, vol. 170, no. 3, 2010, p. 256. Crossref, doi:10.1001/archinternmed.2009.495.
- 23- Yarema, M. C. "Acute Tellurium Toxicity From Ingestion of Metal-Oxidizing Solutions." PEDIATRICS, vol. 116, no. 2, 2005, pp. e319–21. Crossref, doi:10.1542/peds.2005-0172.
- 24- DiPalma, Joseph R. "Bismuth Toxicity, Often Mild, Can Result in Severe Poisonings."

 Emergency Medicine News, vol. 23, no. 3, 2001, p. 16. Crossref, doi:10.1097/00132981-200104000-00012.
- 25- Sundar, Shyam, and Jaya Chakravarty. "Antimony Toxicity." International Journal of Environmental Research and Public Health, vol. 7, no. 12, 2010, pp. 4267–77. Crossref, doi:10.3390/ijerph7124267.
- 26-Technical Glass Products, Inc. "Technical Glass Products: Pressure Calculations."
 Technical Glass Products, 2001, technical glass.com/pressure calculations.

- 27- "Vapor Pressure Calculator [IAP/TU Wien]." Michael Schmid, 25 Sept. 2019, www.iap.tuwien.ac.at/www/surface/vapor_pressure.
- 28-National Institute of Standards and Technology. "Antimony." U.S. Secretary of Commerce on Behalf of the U.S.A, 2018, webbook.nist.gov/cgi/inchi?ID=C7440360&Mask=4.
- 29- Clausius-Clapeyron Equation. 11 Mar. 2021, https://chem.libretexts.org/@go/page/11877.
- 30- "The CALPHAD Methodology." Thermo-Calc Software, 8 Apr. 2021, thermocalc.com/about-us/methodology/the-calphad-methodology.
- 31- "Property Model Calculator." Thermo-Calc Software, 3 May 2021, thermocalc.com/products/thermo-calc/property-model-calculator.
- 32-Haynes, William. CRC Handbook of Chemistry and Physics, 91st Edition (CRC Handbook of Chemistry & Physics). 91st ed., CRC Press, 2010.
- 33-Han, Kyu-Bum, et al. "Enhancement in Surface Mobility and Quantum Transport of Bi2–xSbxTe3–ySey Topological Insulator by Controlling the Crystal Growth Conditions." Scientific Reports, vol. 8, no. 1, 2018. Crossref, doi:10.1038/s41598-018-35674-z.
- 34- "DoITPoMS TLP Library Solidification of Alloys Derivation of the Scheil Equation."

 University of Cambridge, 2004–2020,

 www.doitpoms.ac.uk/tlplib/solidification alloys/scheil derivation.php.
- 35-"Scheil Equations & Solidification Simulations." Thermo-Calc Software, 1 Mar. 2021, thermocalc.com/products/thermo-calc/scheil-solidification-

simulations/#:%7E: text=The%20 Scheil%20 Calculator%20 is%20 a, solidification%20 range e%20 of%20 an%20 alloy.

Work Contributions

Husain F. Alnaser: Wrote the manuscript, Methodology, and analysis. Taylor D. Sparks: research initiation, research supervisor, and data analysis.

Competing Interest

Authors declare no competing interests.